MOF Nanohybrids Hot Paper

How to cite: *Angew. Chem. Int. Ed.* **2023,** *62,* e202301021
International Edition: doi.org/10.1002/anie.202301021
German Edition: doi.org/10.1002/ange.202301021

A Universal Synthesis Strategy for Tunable Metal-Organic Framework Nanohybrids**

Wei Zhang, Michael J. Bojdys, and Nicola Pinna**

Abstract: Metal-organic frameworks (MOFs) with encapsulated nanoparticles (NPs) enjoy a vastly expanded application potential in catalysis, filtration, and sensing. The selection of particular modified core-NPs has yielded partial successes in overcoming lattice mismatch. However, restrictions on the choice of NPs not only limit the diversity, but also affect the properties of the hybrid materials. Here, we show a versatile synthesis strategy using a representative set of seven MOF-shells and six NP-cores that are fine-tuned to incorporate from single to hundreds of cores in mono-, bi-, tri- and quaternary composites. This method does not require the presence of any specific surface structures or functionalities on the pre-formed cores. Our key point is to regulate the diffusion rate of alkaline vapors that deprotonate organic linkers and trigger the controlled MOF-growth and encapsulation of NPs. This strategy is expected to pave the way for the exploration of more sophisticated MOF-nanohybrids.

Introduction

Nanohybrids with multiple components show entirely new physical and chemical phenomena that go beyond those of their constituents in important applications such as light-emitters, catalysts, plasmonic chemistry, sensing and transistors.[1–6] Metal-organic frameworks (MOFs) are uniquely suitable as synthesis platforms for a large variety of multicomponent systems due to their modular and versatile chemistries, and their guest-accessible pore structures.[7–22] To date, MOFs are functionalised predominantly by two strategies: (i) post-synthetic, diffusion-controlled introduction of guests into MOFs by chemical vapor deposition (CVD),[23,24] solid grinding,[25] liquid impregnation,[26] and microphase separation[27] and (ii) by encapsulation of pre-formed guests into a nascent MOF.[28–43]

Both strategies impose severe restrictions on versatility and quality of the targeted nanohybrids. Firstly, pre-formed nanoparticles (NPs) usually require large quantities of capping agents that become trapped in the pore structure and that have detrimental effects on the interface between MOFs and guests.[6,31,35] Secondly, sacrificial template-assisted synthesis usually yields uncontrolled nucleation of polycrystalline MOF-shells around nanoparticle-cores.[36,38] The resulting grain boundaries affect the mass mobility within MOF-shells and decrease the structural integrity of the composites. Thirdly, the conventional strategies fail to deliver the predictable and tunable encapsulation of a target-number of guests. Most syntheses start out with static conditions at fixed concentrations and, hence, yield nanohybrids with either one or many cores. Finally, the vast majority of conventional strategies are valid only for one, specific MOF-shell or functional guest-nanoparticle, which stymies the systematic investigation of MOF-nanohybrids.

A universal synthesis strategy for MOF nanohybrids resolves the long-standing shortcomings of conventional syntheses. This method is based on the rate-controlled deprotonation of organic building blocks by alkaline vapors triggers the heterogeneous nucleation and controlled growth of MOFs in the presence of any number and variety of nanoparticle cores in solution. We control the number of incorporated cores from one to hundreds of by varying the strength of the counter anion from NO_3^- to Cl^-. Unlike the previously reported studies on MOF-composites, this method does not require the presence of any specific surface structures or functionalities on the pre-formed cores. In overview, MOF precursors (metal salts and organic building blocks) are first solubilised and then exposed to a controlled flow of triethylamine (TEA) vapors (Figure 1a). Triethylamine deprotonates an organic building block (e.g., imidazole) which in turn coordinates to a metal ion, and forms the nucleus of the nascent MOF-shell. This heterogeneous nucleation and growth process is compatible with almost any solid substrate, and hence, it enables a universal, combinatorial approach to all possible core–shell combinations. In previous reports, TEA vapor diffusion was employed for synthesizing pure MOF crystals[44–46] or grow-

[*] Dr. W. Zhang, Prof. M. J. Bojdys, Prof. N. Pinna
Institut für Chemie and IRIS Adlershof, Humboldt-Universität zu Berlin
Brook-Taylor-Strasse 2, 12489 Berlin (Germany)
E-mail: zhangweq@hu-berlin.de
nicola.pinna@hu-berlin.de
Prof. M. J. Bojdys
Department of Chemistry, King's College London, Britannia House Guy's Campus
7 Trinity Street, London, SE1 1DB (UK)

[**] A previous version of this manuscript has been deposited on a preprint server (https://doi.org/10.26434/chemrxiv-2022-gl2gt).

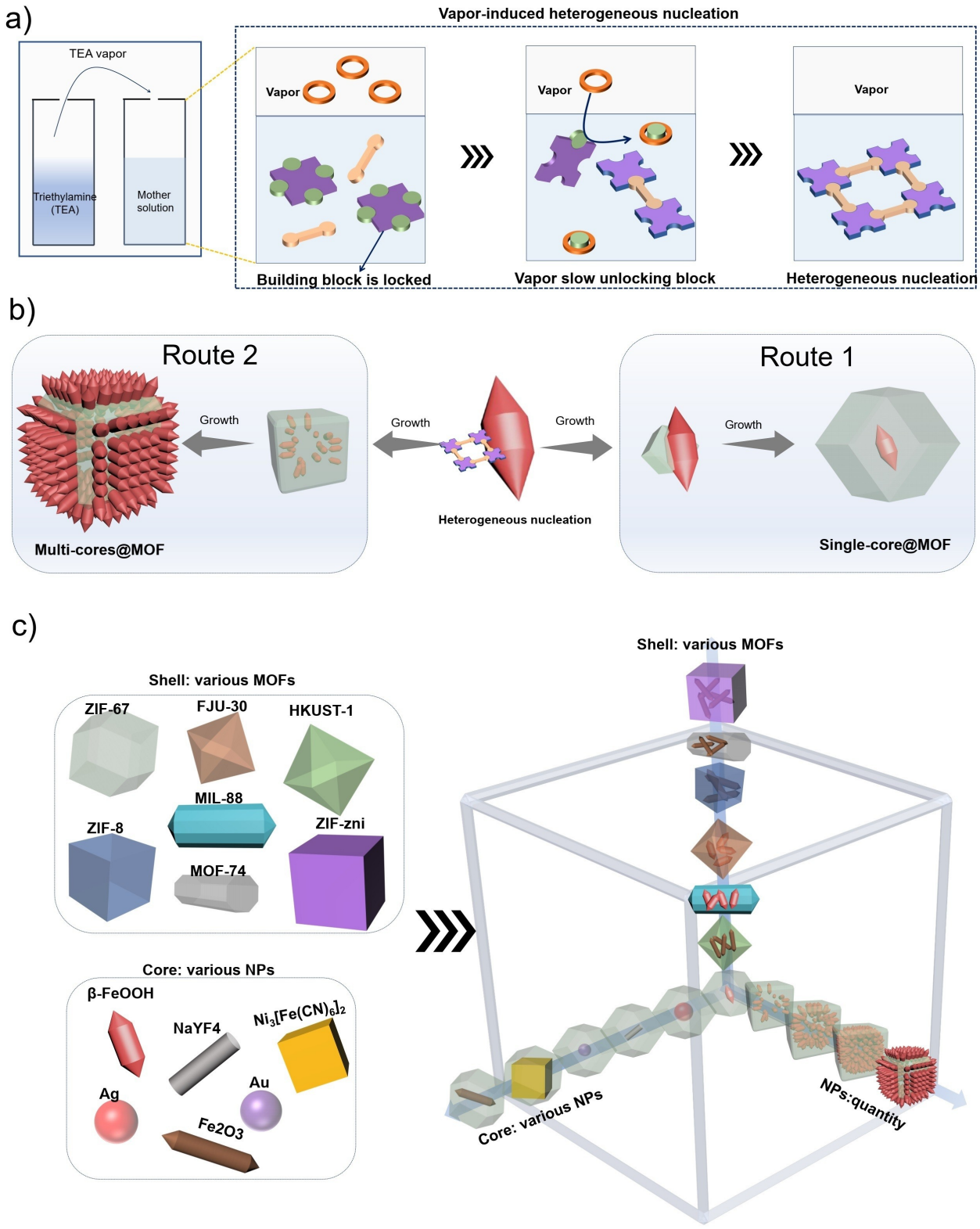

Figure 1. A universal synthesis strategy for various MOF nanohybrids. (a) A proposed set-up consisting of two capped vials in a sealed beaker: one vial contains the mother solution (MOF precursors, nanoparticles (NPs), and solvent). The second vial contains triethylamine solution. TEA vapor diffuses into the mother solution and slowly releases locked ligands and drives heterogeneous nucleation occurring on NPs surface to form MOF nanohybrids. Purple blocks represented deprotonated organic ligands. Green disk represented protons. Pink columns represented metal ions. Orange rings represented triethylamine molecule. (b) Scheme diagram of constructing single-core@MOF and multi-cores@MOF. Strong coordinating anion (Cl^-) can induce formation of multi-cores@MOF and weaker coordinating anion (NO_3^-) can induce formation of single-core@MOF. (c) The 3D models of various MOFs, NPs and the obtained MOF nanohybrids in this work.

ing MOF on substrates to form thin films,[47] or at liquid–gas interface to form membranes[48] and in three-dimensionally connected templates.[49] But no reports have been made on the synthesis of MOF nanohybrids. To illustrate the versatility of this method in construction of nanohybrids, we focus on a set of seven archetypal MOF-shells (ZIF-zni,[50] ZIF-8,[9] ZIF-67,[28] FJU-30,[51] MIL-88(Fe),[52] HKUST-1,[15] and MOF-74(Co)[53]) and six commonly-used core species (Ag, Au, $NaYF_4$, β-FeOOH, Fe_2O_3 and $Ni_3[Fe(CN)_6]_2$). (Figure 1b,1c) This report demonstrates that (i) we can overcome the lattice mismatch between the various shells and cores, (ii) we form high-quality, single-crystalline MOF-shells, and (iii) we can precisely control the number and variety of cores within individual MOF-nanoparticles. The successful growth of MOF-shells around various, as-received cores using simple, vapor-assisted deprotonation opens a new and universal route for the development of a future generation of MOF-nanohybrids for plasmonic chemistry, catalysis, and sensing.

Results and Discussion

To facilitate the vapor-assisted deprotonation and growth of the target MOF-shells, we have devised a simple set-up consisting of two capped vials in a sealed beaker (Figure 1a and S1): one vial contains the mother solution (MOF precursors, nanoparticles, and solvent), and it is closed by a cap with one hole (1 mm diameter). The second vial contains ethanolic solution of triethylamine (volume ratios of triethylamine/ethanol are listed in Table S1), and a cap punctured by three holes (1 mm diameter each). In a typical experiment, the two vials were left in close proximity under sealed atmosphere and room temperature for 8 hours. All obtained MOF-shells were subsequently washed with ethanol for several times and identified by phase-matching of powder X-ray diffraction (PXRD) data (Figure S2).

In the following, we select as an example the nanohybrid based on a ZIF-67 shell containing multiple β-FeOOH nanoparticle cores (denoted as multi-β-FeOOH@ZIF-67) to explain the encapsulation process. Nanorods of β-FeOOH are ideal cores for the construction of nanohybrids, since their surfaces are surfactant-free. In a typical synthesis, cobalt chloride (9.5 mg, 4 mM), 2-methylimidazole (8.2 mg, 10 mM), and β-FeOOH (0.25 mL, 2 mg L^{-1}) are dissolved in a total volume of 10 mL of ethanol to form the mother solution. Subsequently, we seal one vial of the mother solution and one vial of triethylamine solution (volume ratio TEA/EtOH of 1:3) in a 500 mL beaker (Figure S1). In the absence of a base, 2-methylimidazole ($pK_a = 14.4$)[54] is predominantly present in its protonated form (ethanol $pK_a = 16.0$). Since the initial concentration of 2-methylimidazol anions (approx. 10^{-8} mol L^{-1}) is low, nucleation of ZIF-67 does not take place (Figure S1). As triethylamine ($pK_a = 7.73$)[55] gradually diffuses into the mother solution, the equilibrium shifts to the formation of 2-methylimidazole anions that drive heterogeneous nucleation of ZIF-67 on the surface of β-FeOOH (Figure 2a and S3). Transmission electron microscopy (TEM), high-angle annular dark field (HAADF) scanning transmission electron microscopy (STEM), and energy-dispersive X-ray (EDX) spectroscopy on the multi-β-FeOOH@ZIF-67 composites show that β-FeOOH nanorods are uniformly distributed throughout the entire ZIF-67 shell (Figure 2a).

We conducted a series of control experiments to gain insight into the encapsulation process. We adjusted the rate of diffusion of triethylamine by changing the volume ratios of TEA/Ethanol (from 2:10, 3:9, 4:8 to 12:0). At a ratio below 3:9, β-FeOOH nanorods are successfully encapsulated into ZIF-67 shells to form the multi-β-FeOOH@ZIF-67 composite (Figure S4a–4d). In the regime of low triethylamine concentrations, more β-FeOOH nanorods will be incorporated per core–shell particle. When the volume ratio increased to 4:8 (Figure S4e–4f), the size distribution of core–shell composites becomes broad which indicates multiple nucleation events and an uncontrolled growth and encapsulation process. In the extreme case when pure triethylamine is used, we observe homogeneous nucleation of pure ZIF-67 crystals as the major product (Figure S4g–4h). We used the ratios of weight of the inorganic particles (after MOF dissolution) to weight of primal nanohybrids and the atomic ratio of Fe/Co by EDS spectrum to simultaneously evaluate the number of β-FeOOH nanorods per ZIF-67 ($Co(Hmim)_2$) particle. As we increase the volume ratio of TEA/Ethanol, we observe ratios of weight of the inorganic particles has been reduced from 39.2 % to 4.1 %. Meanwhile, the EDS spectrum show that the ratio of Fe/Co decreases from 1.6 (β-FeOOH, 40 wt% in hybrid) to nearly 0 (Figure S5). In addition to changing volume ratios of TEA, the diffusion rate can be regulated by varying the number of holes in TEA solution vial as well (Figure S6). As the number of holes increases from two to four, the size of nanohybrids decreases, and internal β-FeOOH loads are also reduced. These results demonstrate the importance of slow diffusion/deprotonation to achieve a heterogeneous nucleation and a "quasi-living" growth of ZIF-67 shells around cores.

In our example, the multi-β-FeOOH@ZIF-67 size grew from 500 nm to 4 μm when the concentration of the metal salt ($CoCl_2$) was increased from 2 mM to 8 mM, respectively (under commensurate scaling of all components in the mother solution) (Figure S7). Using an appropriate TEA/EtOH ratio (of 3:9), we observe the uniform encapsulation of a multitude of β-FeOOH nanorods (at a Fe/Co ratio of 0.9) for all ZIF-67 shells obtained at various concentrations. These results show that the size of multi-β-FeOOH@ZIF-67 nanohybrids can be easily tuned by changing the initial concentration of the precursors.

We increased the concentration of β-FeOOH nanorods from 10 to 250 mg L^{-1} while keeping other parameters constant. TEM images show an increased number of β-FeOOH nanorods within the uniformly shaped shells (Figure 2b and S8). This qualitative observation is verified by a quantitative increase of Fe/Co ratios from 0.13 to 1.6 as the concentration of cores is increased (Figure 2c and S9). Given a slow nucleation of the shells, the number of β-FeOOH nanorods per ZIF-67 particle increases approximately linearly with the initial core concentration. During the growth

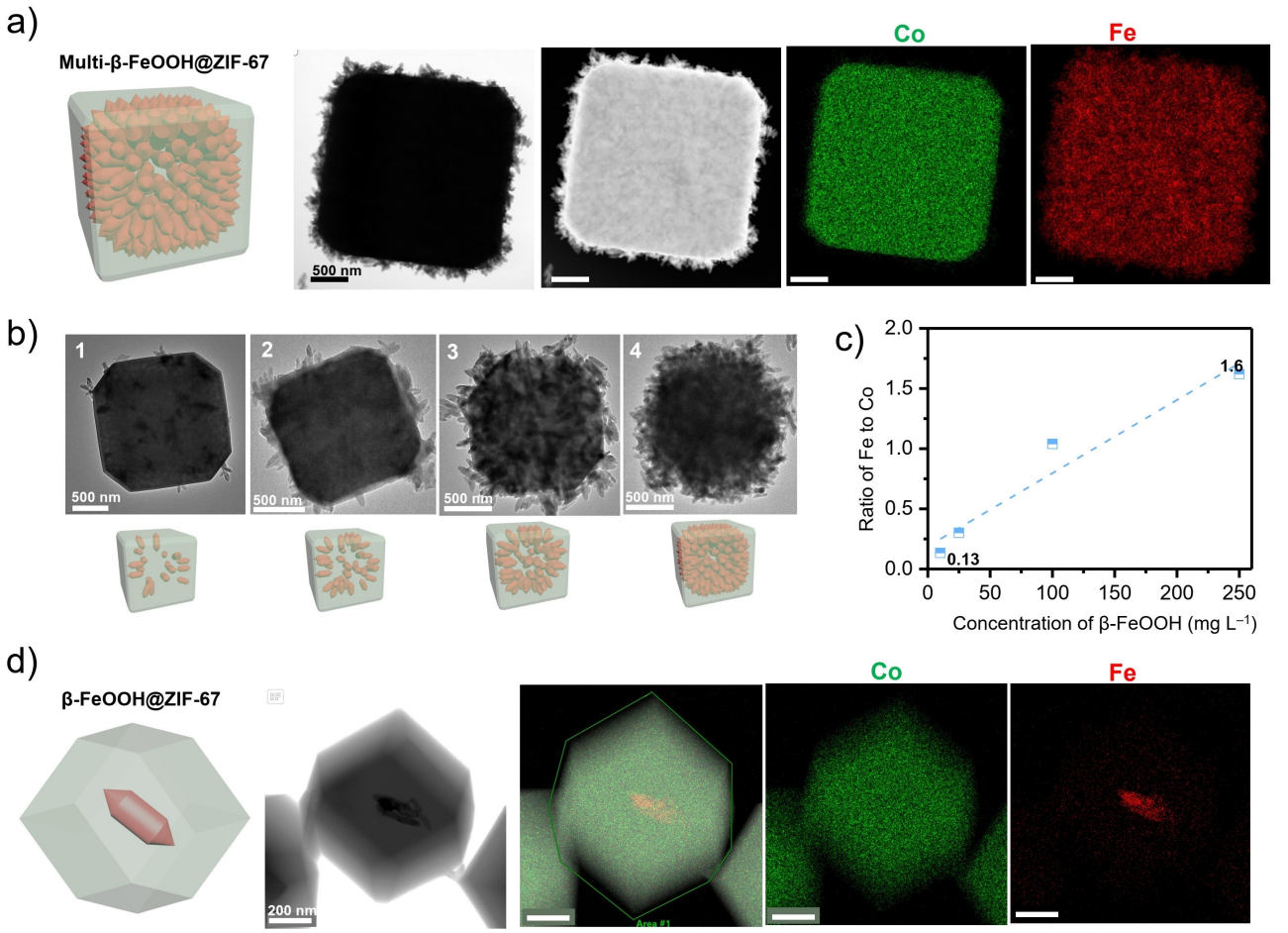

Figure 2. Structure characterization of multi-β-FeOOH@ZIF-67 and β-FeOOH@ZIF-67. (a) The 3D model, TEM image, STEM image and corresponding element mapping images of multi-β-FeOOH@ZIF-67 nanohybrids. The scale bar is 500 nm. (b) TEM images and 3D models of multi-β-FeOOH@ZIF-67 obtained at different initial β-FeOOH concentrations. **1**:10 mg L^{-1}; **2**:25 mg L^{-1}; **3**:100 mg L^{-1}; **4**: 250 mg L^{-1}. (c) The ratio of Fe to Co as a function of initial concentration of β-FeOOH nanorod. (d) The 3D model, TEM image and corresponding element mapping images of β-FeOOH@ZIF-67. The scale bar is 200 nm.

process, β-FeOOH nanorods continuously adsorb onto the ZIF-67 crystal surface and became encapsulated in subsequent stages of growth. Hence, we are able to achieve multi-β-FeOOH@ZIF-67 nanohybrids with core-contents ranging from 5% to 40% simply by adjusting the initial core concentration.

To achieve the encapsulation of a singular core-particle, we had to make sure that the MOF-shell grows with sufficient speed while at the same time producing single-crystalline MOF-domains of comparable size. Following our deliberations on growth and size control above, we disregarded an approach using simple concentration-dependent diffusion kinetics, since we needed to ensure MOF-shell undergo heterogeneous nucleation and relatively fast growth process. MOF-growth is decisively influenced by the strong interactions between chloride anions and Co^{2+} ions in the solvated metal-salt precursor ($Co[(EtOH)_4Cl_2]$).[56] We varied the MOF-growth kinetics by using $Co(NO_3)_2$ instead of $CoCl_2$ (Figure S10) as the metal salt precursor, effectively substituting a small, strongly coordinating anion (Cl^-) by a delocalised, weaker coordinating anion (NO_3^-). Similar to $CoCl_2$ system, we sealed the mother solution containing equivalent concentrations of $Co(NO_3)_2$, 2-methylimidazole and β-FeOOH nanorods in our vapor-diffusion set-up. TEM images of obtained β-FeOOH@ZIF-67 nanohybrids show the successfully encapsulation of individual β-FeOOH nanorods within discrete shells of ZIF-67 (Figure 2d and S11–12). The size of the core–shell nanohybrid particles is approx. 500 nm with a characteristic rhombic dodecahedron shape indicative of ZIF-67. The HAADF-STEM imaging and EDX elemental maps of a single β-FeOOH@ZIF-67 particle indicate the successful synthesis of the core–shell structure (Figure 2d, Figure S13).

Finally, we used the LaMer-type growth model to qualitatively evaluate the different processes of nucleation and growth of the two MOF nanohybrids, β-FeOOH@ZIF-67 and multi-β-FeOOH@ZIF-67 (Figure S14a).[30] For single β-FeOOH@ZIF-67, the metal precursor $Co(NO_3)_2$ provides free cobalt cations readily at the onset of the reaction (Figure S14b). With the diffusion of triethylamine into the mother solution, 2-methylimidazole anion concentration increases slowly (Figure S14c). When the concentration

required for heterogeneous nucleation is reached, growth of ZIF-67 occurs preferentially on the surface of β-FeOOH (Figure S15), since the nucleation threshold is lower on a solid surface (Figure S14a). Subsequently, free Co^{2+} cations and 2-methylimidazole anions rapidly attach onto these primary nuclei leading to further growth of the MOF-shell into single β-FeOOH@ZIF-67 nanohybrids (Figure S15a). Using $CoCl_2$, the concentration of free cobalt cations is very low throughout the reaction (Figure S10, S14b). TEA vapors gradually diffuse into the mother solution forming 2-methylimidazole anions. When the nucleation threshold is reached, fewer MOF-nuclei form on the surfaces of β-FeOOH compared to the $Co(NO_3)_2$ system. Due to competing Cl^- anions in the solution, the nascent surfaces of ZIF-67 nuclei are less stable. Absorption of β-FeOOH onto such a fresh ZIF-67 surface leads to its stabilization (Figure S15b). As a result, the β-FeOOH-MOF nuclei gradually agglomerate into micron-sized multi-β-FeOOH@ZIF-67 nanohybrids. Their recognizable equilibrium morphology (Figure S16) and epitaxial growth results (Figure S17) suggest the formation of single crystal ZIF-67 in above cases.

In the example above, the formation of the composites does not rely on the presence of specific surface species or on a lattice match between the core and the shell. Therefore, it is possible to extend our method to a multitude of core–shell systems. We selected inorganic nanoparticles with different functional groups, and with different morphologies and sizes including surfactant-free Fe_2O_3 ellipsoids, tannic acid stabilized Ag NPs, oleic acid modified $NaYF_4$ NPs, PVP stabilized Au NPs and citrate capped $Ni_3[Fe(CN)_6]_2$ nanocubes to synthesize the corresponding ZIF-67 nanohybrids (Figure S18). TEM images of core@ZIF-67 nanohybrids show the successful synthesis of core–shell structures that are independent of the chemistry and morphology of the core (Figure 3 and S19–20). As in our initial example, using $Co(NO_3)_2$ as precursor results in the encapsulation of only one (or few) NP-cores within individual ZIF-67-shells (Figure 3a). As expected, $CoCl_2$ yields core–shell nanohybrids with larger core-content per particle (Figure 3b).

Since the formation of the core–shell composites is fully independent of the core, we designed more complicated structures combining two, three and four types of cores into one MOF-shell. In the growth process, ZIF-67 shells encapsulate any colloidally stable nanoparticle. Consequently, we obtained complex MOF hybrids as binary- (*β-FeOOH, $NaYF_4$*@ZIF-67), tertiary- (*β-FeOOH, $NaYF_4$, Au*@ZIF-67) and quaternary composites (*β-FeOOH, $NaYF_4$, Au, Ag*@ZIF-67) using our method (Figure 3c and S21–23). The corresponding EDX elemental analysis and mapping show that different types of inorganic nanoparticles are uniformly distributed in micron-sized ZIF-67 shells (Figure 3c, Figure S21–23).

As mentioned before, the ratios of triethylamine/ethanol solutions are used to regulate the diffusion rates of TEA, and therefore influencing the deprotonation of organic ligands. A lower ratio of triethylamine/ethanol solutions corresponds to a slower deprotonation process. In addition, the ratios of ligands to metal precursors affect the MOF growth as well. The excess ligand linker usually increases

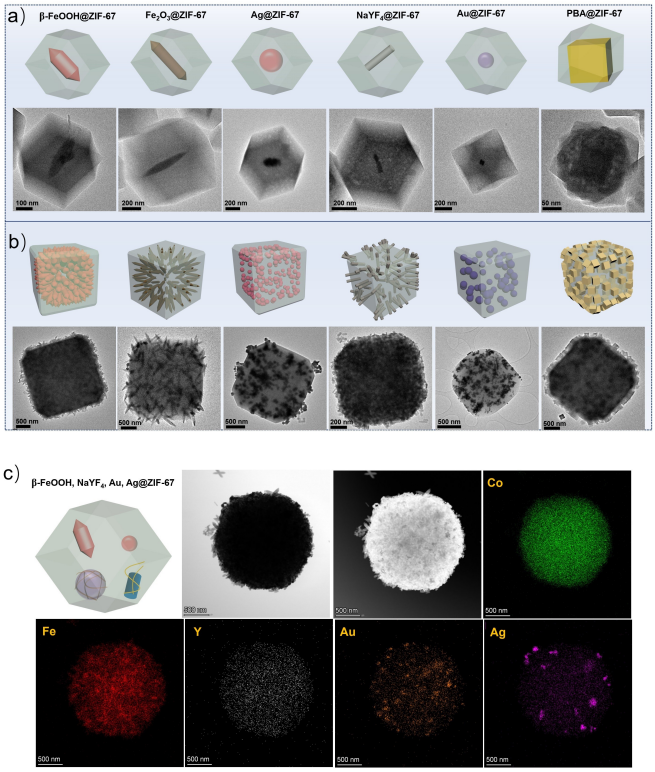

Figure 3. TEM images of ZIF-67 nanohybrids that encapsulate different types and contents of nanocrystals. (a) The 3D models and TEM images of ZIF-67 nanohybrids that contain surfactant-free β-FeOOH nanorod, surfactant-free Fe_2O_3, tannic acid stabilized Ag, contain oleic acid stabilized $NaYF_4$, PVP stabilized Au and sodium citrate stabilized $Ni_3[Fe(CN)_6]_2$.These ZIF-67 nanohybrids are synthesized by using $Co(NO_3)_2$ as metal precursor. (b) The 3D models and TEM images of ZIF-67 nanohybrids that contain numerous nanoparticles. These ZIF-67 nanohybrids are synthesized by using $CoCl_2$ as metal precursor. (c) The 3D model, TEM image and corresponding element mapping images of β-FeOOH, $NaYF_4$, Au, Ag@ZIF-67 composite (four types of nanocrystals) that contain surfactant-free β-FeOOH nanorod, oleic acid stabilized $NaYF_4$, PVP stabilized Au and tannic acid stabilized Ag.

the formation of metal-ligand complexation and therefore improving rate of crystallization and nucleation. Slower growth rate of MOF facilitates crystal growth and engulfment of more nanoparticles within per particles. Therefore, we will try to optimize rational reaction parameters to widen the scope of our method to encompass different MOF-shells. We selected ZIF-8 as an excellent starting-candidate since it has the same crystal structure as ZIF-67, and it consist of of Zn^{2+} cations and 2-methylimidazole anions.[9] Using $ZnCl_2$ as the metal precursor, we obtained various micron-sized nanohybrids with ZIF-8 shells (Figure 4 and S24–25). Subsequently, we chose structurally very different systems FJU-30 ($Zn_5(C_2H_2N_3)_6Cl_4$) and ZIF-zni ($Zn(IM)_2$). FJU-30 and ZIF-zni are composed of Zn^{2+} cations and 1H–1,2,3-triazole anions and imidazole anions, respectively[50,51]—both organic building blocks are deprotonated by the stronger base, triethylamine. The TEM images show the successful synthesis of nanohybrids with shells of FJU-30 and ZIF-zni (Figure 4 and S26–28). With N-containing ligands exhaus-

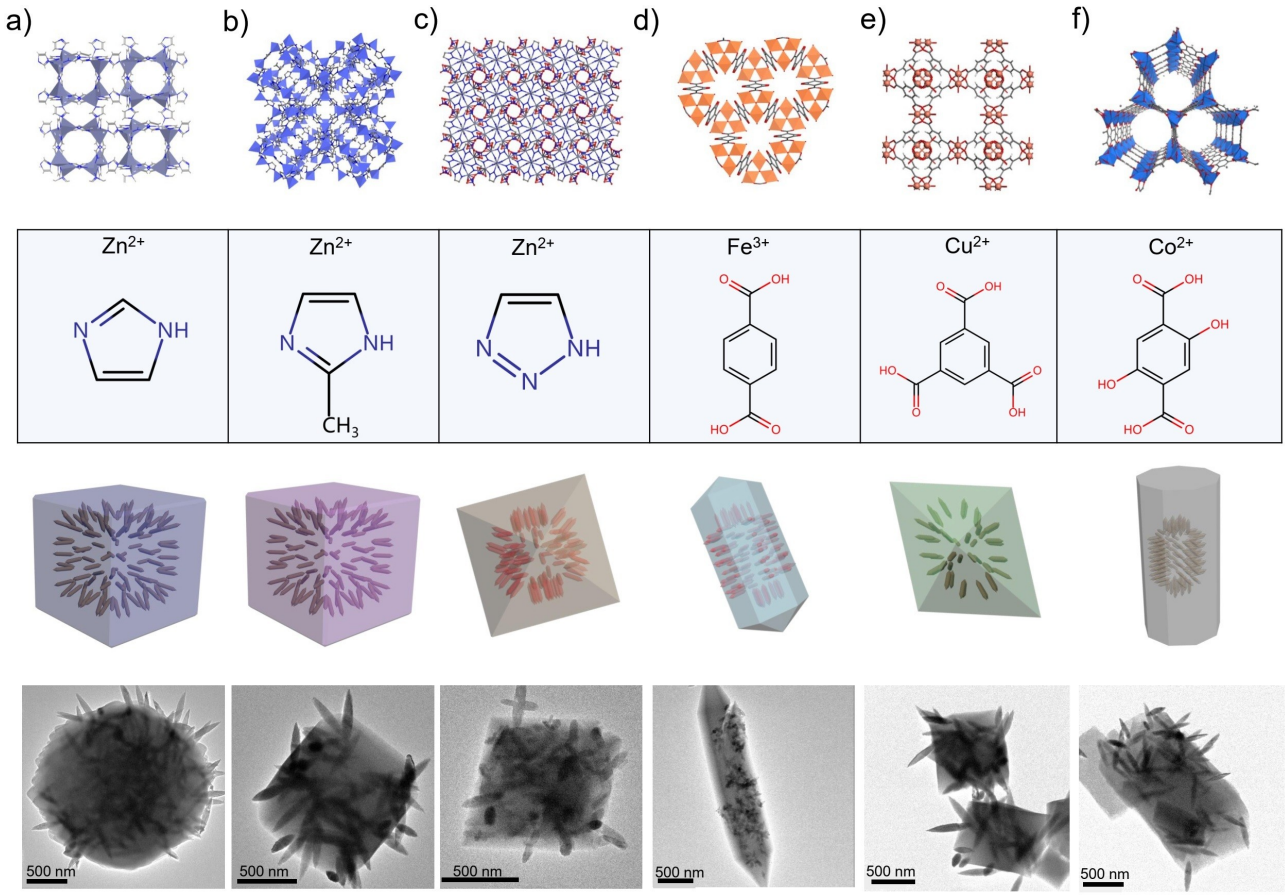

Figure 4. (a) The crystal structure of ZIF-zni, components of ZIF-zni, 3D model and TEM images of multi-Fe_2O_3@ZIF-zni nanohybrids (From top to bottom, respectively). (b) The crystal structure of ZIF-8, components of ZIF-8, 3D model and TEM images of multi-Fe_2O_3@ZIF-8 nanohybrids. (c) The crystal structure of FJU-30, components of FJU-30, 3D model and TEM images of multi-β-FeOOH@FJU-30 nanohybrids. (d) The crystal structure of MIL-88, components of MIL-88, 3D model and TEM images of multi-β-FeOOH @MIL-88 nanohybrids. (e) The crystal structure of HKUST-1, components of HKUST-1, 3D model and TEM images of multi-Fe_2O_3@HKUST-1 nanohybrids. (f) The crystal structure of MOF-74, components of MOF-74, 3D model and TEM images of multi-Fe_2O_3@MOF-74 nanohybrids.

tively covered, we apply our method to O-containing organic building blocks. Here, we selected MIL-88 (from Fe^{3+} and BDC (1,4-Benzenedicarboxylate)),[52] HKUST-1 (from Cu^{2+} and BTC (1,3,5-benzenetricarboxylate))[15] and Co-MOF-74 (from Co^{2+} and DOBDC (2,5-dioxido-1,4-benzenedicarboxylate))[47] as the shells into which we successfully incorporated various NPs as cores (Figure 4 and Figure S29–31). In addition to ethanol, various MOF nanohybrids can be obtained as well via using DMF or isopropanol as solvents (Figure S32–34). Our results unambiguously demonstrate that our proposed method is a powerful synthesis tool with a very broad scope for the synthesis of well-defined, tailored, and chemically extremely versatile MOF nanohybrids.

Conclusion

Using this uniquely versatile method of vapor-assisted deprotonation and nucleation of MOFs around various NP-cores, we have obtained a multitude of nanohybrids from seven different MOF shells (ZIF-zni, ZIF-8, ZIF-67, NJU-30, MIL-88(Fe), HKUST-1 and MOF-74(Co)) and six core species (Ag, Au, $NaYF_4$, β-FeOOH, Fe_2O_3 and $Ni_3[Fe(CN)_6]_2$). The rate of diffusion of triethylamine vapors controls the deprotonation process of organic building blocks, and thus allows precise and unprecedented control over the growth dynamics and compositions of core–shell nanohybrids. The slow deprotonation process favours heterogeneous nucleation at the surfaces of colloidal nanoparticles—independent of their chemistries, structures and morphologies. We can tailor the precise number of encapsulated core-particles from one to hundreds by (i) adjusting the rate of nucleation and by (ii) tuning the coordination environment of the metal precursors. As a result, our method is applicable to any kind of core-nanoparticle and various MOF-shells that can be combined into simple and complex (binary, tertiary-, and quaternary) composite systems. This method provides a powerful tool for the design and synthesis of the future generation of MOF-based core–shell nanohybrids.

Acknowledgements

W.Z thanks the Alexander von Humboldt Foundation, Bonn, Germany, for a postdoctoral fellowship and research grants. Open Access funding enabled and organized by Projekt DEAL.

Conflict of Interest

The authors declare no conflict of interest.

Data Availability Statement

The data that support the findings of this study are available from the corresponding author upon reasonable request.

Keywords: Hybrid Materials · Metal Organic Frameworks · Nanocrystals · Organic–Inorganic Nanostructures

[1] B. S. Mashford, M. Stevenson, Z. Popovic, C. Hamilton, Z. Zhou, C. Breen, J. Steckel, V. Bulovic, M. Bawendi, S. Coe-Sullivan, *Nat. Photonics* **2013**, *7*, 407–412.
[2] B. Lim, M. Jiang, P. H. Camargo, E. C. Cho, J. Tao, X. Lu, Y. Zhu, Y. Xia, *Science* **2009**, *324*, 1302–1305.
[3] X. Yang, Y. Liu, S. H. Lam, J. Wang, S. Wen, C. Yam, L. Shao, J. Wang, *Nano Lett.* **2021**, *21*, 8205–8212.
[4] M. S. Yao, J. W. Xiu, Q. Q. Huang, W. H. Li, W. W. Wu, A. Q. Wu, L. A. Cao, W. H. Deng, G. E. Wang, G. Xu, *Angew. Chem. Int. Ed.* **2019**, *58*, 14915–14919.
[5] H. Tada, T. Mitsui, T. Kiyonaga, T. Akita, K. Tanaka, *Nat. Mater.* **2006**, *5*, 782–786.
[6] G. Lu, S. Li, Z. Guo, O. K. Farha, B. G. Hauser, X. Qi, Y. Wang, X. Wang, S. Han, X. Liu, *Nat. Chem.* **2012**, *4*, 310–316.
[7] Q. L. Zhu, Q. Xu, *Chem. Soc. Rev.* **2014**, *43*, 5468–5512.
[8] M. Eddaoudi, H. Li, O. M. Yaghi, *J. Am. Chem. Soc.* **2000**, *122*, 1391–1397.
[9] K. S. Park, Z. Ni, A. P. Côté, J. Y. Choi, R. Huang, F. J. Uribe-Romo, H. K. Chae, M. O'Keeffe, O. M. Yaghi, *Proc. Natl. Acad. Sci. USA* **2006**, *103*, 10186–10191.
[10] S. Horike, S. Shimomura, S. Kitagawa, *Nat. Chem.* **2009**, *1*, 695–704.
[11] Y. Sakata, S. Furukawa, M. Kondo, K. Hirai, N. Horike, Y. Takashima, H. Uehara, N. Louvain, M. Meilikhov, T. Tsuruoka, *Science* **2013**, *339*, 193–196.
[12] M. Zhao, K. Yuan, Y. Wang, G. Li, J. Guo, L. Gu, W. Hu, H. Zhao, Z. Tang, *Nature* **2016**, *539*, 76–80.
[13] X. Yang, S. Yuan, L. Zou, H. Drake, Y. Zhang, J. Qin, A. Alsalme, H. C. Zhou, *Angew. Chem. Int. Ed.* **2018**, *57*, 3927–3932.
[14] J. Liu, C. Wöll, *Chem. Soc. Rev.* **2017**, *46*, 5730–5770.
[15] A. Carné-Sánchez, I. Imaz, M. Cano-Sarabia, D. Maspoch, *Nat. Chem.* **2013**, *5*, 203–211.
[16] I. Stassen, M. Styles, G. Grenci, H. V. Gorp, W. Vanderlinden, S. D. Feyter, P. Falcaro, D. D. Vos, P. Vereecken, R. Ameloot, *Nat. Mater.* **2016**, *15*, 304–310.
[17] R. Dong, P. Han, H. Arora, M. Ballabio, M. Karakus, Z. Zhang, C. Shekhar, P. Adler, P. S. Petkov, A. Erbe, *Nat. Mater.* **2018**, *17*, 1027–1032.
[18] D. Esken, S. Turner, O. I. Lebedev, G. Van Tendeloo, R. A. Fischer, *Chem. Mater.* **2010**, *22*, 6393–6401.
[19] S. Dai, A. Tissot, C. Serre, *Adv. Energy Mater.* **2021**, 2100061.
[20] Q. Yang, Q. Xu, H. L. Jiang, *Chem. Soc. Rev.* **2017**, *46*, 4774–4808.
[21] J. Yu, C. Mu, B. Yan, X. Qin, C. Shen, H. Xue, H. Pang, *Mater. Horiz.* **2017**, *4*, 557–569.
[22] J. Li, S. Cheng, Q. Zhao, P. Long, J. Dong, *Int. J. Hydrogen Energy* **2009**, *34*, 1377–1382.
[23] S. Hermes, M. K. Schröter, R. Schmid, L. Khodeir, M. Muhler, A. Tissler, R. W. Fischer, R. A. Fischer, *Angew. Chem. Int. Ed.* **2005**, *44*, 6237–6241.
[24] F. Schröder, D. Esken, M. Cokoja, M. W. Van Den Berg, O. I. Lebedev, G. Van Tendeloo, B. Walaszek, G. Buntkowsky, H.-H. Limbach, B. Chaudret, *J. Am. Chem. Soc.* **2008**, *130*, 6119–6130.
[25] H. L. Jiang, B. Liu, T. Akita, M. Haruta, H. Sakurai, Q. Xu, *J. Am. Chem. Soc.* **2009**, *131*, 11302–11303.
[26] H. R. Moon, J. H. Kim, M. P. Suh, *Angew. Chem. Int. Ed.* **2005**, *44*, 1261–1265.
[27] A. Aijaz, A. Karkamkar, Y. J. Choi, N. Tsumori, E. Rönnebro, T. Autrey, H. Shioyama, Q. Xu, *J. Am. Chem. Soc.* **2012**, *134*, 13926–13929.
[28] J. Tang, R. R. Salunkhe, J. Liu, N. L. Torad, M. Imura, S. Furukawa, Y. Yamauchi, *J. Am. Chem. Soc.* **2015**, *137*, 1572–1580.
[29] W. Zhang, Y. Li, C. Shi, R. Qi, M. Hu, *J. Am. Chem. Soc.* **2021**, *143*, 6447–6459.
[30] J. W. Osterrieth, D. Wright, H. Noh, C.-W. Kung, D. Vulpe, A. Li, J. E. Park, R. P. Van Duyne, P. Z. Moghadam, J. J. Baumberg, *J. Am. Chem. Soc.* **2019**, *141*, 3893–3900.
[31] C. Wang, K. E. DeKrafft, W. Lin, *J. Am. Chem. Soc.* **2012**, *134*, 7211–7214.
[32] K. Liang, J. J. Richardson, C. J. Doonan, X. Mulet, Y. Ju, J. Cui, F. Caruso, P. Falcaro, *Angew. Chem. Int. Ed.* **2017**, *56*, 8510–8515.
[33] P. Hu, J. Zhuang, L. Y. Chou, H. K. Lee, X. Ling, Y. C. Chuang, C. K. Tsung, *J. Am. Chem. Soc.* **2014**, *136*, 10561–10564.
[34] Y. Gu, Y. N. Wu, L. Li, W. Chen, F. Li, S. Kitagawa, *Angew. Chem. Int. Ed.* **2017**, *56*, 15658–15662.
[35] J. Zhou, P. Wang, C. Wang, Y. T. Goh, Z. Fang, P. B. Messersmith, H. Duan, *ACS Nano* **2015**, *9*, 6951–6960.
[36] Q. Yang, W. Liu, B. Wang, W. Zhang, X. Zeng, C. Zhang, Y. Qin, X. Sun, T. Wu, J. Liu, F. Huo, J. Lu, *Nat. Commun.* **2017**, *8*, 14429.
[37] G. Lee, S. Lee, S. Oh, D. Kim, M. Oh, *J. Am. Chem. Soc.* **2020**, *142*, 3042–3049.
[38] W. W. Zhan, Q. Kuang, J. Z. Zhou, X. J. Kong, Z. X. Xie, L. S. Zheng, *J. Am. Chem. Soc.* **2013**, *135*, 1926–1933.
[39] H. Liu, L. Chang, C. Bai, L. Chen, R. Luque, Y. Li, *Angew. Chem. Int. Ed.* **2016**, *55*, 5019–5023.
[40] Y. Yun, H. Sheng, K. Bao, L. Xu, Y. Zhang, D. Astruc, M. Zhu, *J. Am. Chem. Soc.* **2020**, *142*, 4126–4130.
[41] L. He, Y. Liu, Y. Liu, J. Liu, Y. Xiong, J. Zheng, Z. Tang, *Angew. Chem. Int. Ed.* **2013**, *52*, 3741–3745.
[42] M. Zhao, K. Deng, L. He, Y. Liu, G. Li, H. Zhao, Z. Tang, *J. Am. Chem. Soc.* **2014**, *136*, 1738–1741.
[43] B. Rungtaweevoranit, J. Baek, J. R. Araujo, B. S. Archanjo, K. M. Choi, O. M. Yaghi, G. A. Somorjai, *Nano Lett.* **2016**, *16*, 7645–7649.
[44] H. Li, M. Eddaoudi, M. O'Keeffe, O. M. Yaghi, *Nature* **1999**, *402*, 276–279.
[45] H. Li, C. E. Davis, T. L. Groy, D. G. Kelley, O. M. Yaghi, *J. Am. Chem. Soc.* **1998**, *120*, 2186–2187.
[46] R. Li, Y. P. Yuan, L. G. Qui, W. Zhang, J. F. Zhu, *Small* **2012**, *8*, 225–230.
[47] K. Yuan, T. Song, X. Zhu, B. Li, B. Han, L. Zheng, J. Li, X. Zhang, W. Hu, *Small* **2019**, *15*, 1804845.
[48] H. Lu, S. Zhu, *Eur. J. Inorg. Chem.* **2013**, 1294–1300.

[49] R. R. Gonte, P. Deb, K. Balasubramanian, *J. Polym.* **2013**, *2013*, 684584.
[50] J. C. Tan, T. D. Bennett, A. K. Cheetham, *Proc. Natl. Acad. Sci. USA* **2010**, *107*, 9938–9943.
[51] Y. Ye, X. Wu, Z. Yao, L. Wu, Z. Cai, L. Wang, X. Ma, Q. H. Chen, Z. Zhang, S. Xiang, *J. Mater. Chem. A* **2016**, *4*, 4062–4070.
[52] C. Serre, F. Millange, S. Surblé, G. Férey, *Angew. Chem. Int. Ed.* **2004**, *43*, 6285–6289.
[53] A. R. Millward, O. M. Yaghi, *J. Am. Chem. Soc.* **2005**, *127*, 17998–17999.
[54] M. Erkartal, U. Erkilic, B. Tam, H. Usta, O. Yazaydin, J. T. Hupp, O. K. Farha, U. Sen, *Chem. Commun.* **2017**, *53*, 2028–2031.
[55] A. V. Rayer, K. Z. Sumon, L. Jaffari, A. Henni, *J. Chem. Eng. Data* **2014**, *59*, 3805–3813.
[56] G. H. Ayres, B. V. Glanville, *Anal. Chem.* **1949**, *21*, 930–934.

Manuscript received: January 19, 2023
Accepted manuscript online: March 6, 2023
Version of record online: April 18, 2023